J Mater Sci (2010) 45:3490–3496
DOI 10.1007/s10853-010-4380-0

# Enhancing mechanical and fracture properties of sandwich composites using nanoparticle reinforcement

**Justin K. Stewart · Hassan Mahfuz · Leif A. Carlsson**

Received: 8 December 2009 / Accepted: 3 March 2010 / Published online: 16 March 2010


**Abstract** Polyurethane (PU) foam is reinforced with SiC nanoparticles to develop core materials for sandwich composites. Isocyanate component (Part A) of PU foam was dispersed with SiC nanoparticles, and then mixed with polyol (Part B) to manufacture nanophased core materials. Nanoparticle reinforcement varied from 0.1 to 2.0 wt% of the total polymer. Both pristine and silane functionalized SiC nanoparticles were used in the investigation. Nanophased foams were tested in compression and flexure to determine the mechanical properties. Fracture toughnesses $K_{IC}$ and $G_{IC}$ were determined using the SENB test. Sandwich panels were fabricated and tested for face-core debond fracture toughness using the tilted sandwich debond test. The study has revealed that reinforcement of the foam by pristine nanoparticles substantially enhances mechanical properties but degrades fracture toughness. This loss in fracture toughness, however, may be recovered with the use of functionalized nanoparticles. Small concentrations (0.1–0.2 wt%) of functionalized nanoparticles provided large improvement in debond fracture toughness of sandwich specimens.

## Introduction

Reinforcement of polyurethane (PU) foam with nanoparticles has been extensively studied in recent years [1–9]. In most cases, the main emphasis was on the improvement of mechanical and thermal properties of foam while in other cases, nanophased foam was used as core material in a sandwich construction and the mechanical behavior of sandwich was evaluated. Several nanoparticles were examined; SiC, $TiO_2$, carbon nanotubes (CNTs), carbon nanofibers (CNFs), and nanoclay, etc. The concentration of particles ranged between 0.5 and 3.0 wt%. Gain in mechanical properties such as strength, stiffness, and impact strength varied with the type and concentration of particle. The improvement in properties was noticeable and provided impetus for further research in this area.

While there are several studies, e.g., [10–18] of the fracture toughness of foams, there are very few [19–21] dealing with those of nanophased foams and sandwich panels. A sandwich structure provides very high stiffness per unit weight due to the combination of two stiff face sheets separated by a low-density core. If a debond is introduced in such structure, its structural stiffness may be substantially reduced because of the loss of shear and tension transfer between face and core. Consequently, face/core debond may pose a substantial threat to the integrity of a sandwich structure [22, 23]. Determination of debond fracture toughness of a sandwich composite is therefore a critical criterion for its structural integrity.

Dispersed nanoparticles could play an important role in controlling the fracture as these particles are embedded within the polymer at the nanoscale. Mechanisms such as crack-pinning and particle–polymer debonding can contribute to energy absorption during the fracture process [24]. This energy absorption feature of nanoparticles was utilized in the current investigation by dispersing SiC nanoparticles into PU foams. Compression, flexure, and SENB tests were conducted on nanophased foams to determine mechanical properties and fracture toughnesses.

J. K. Stewart
Tyco International, Boca Raton, FL 33486, USA

H. Mahfuz (✉) · L. A. Carlsson
Nanocomposites Laboratory, Department of Ocean and Mechanical Engineering, Florida Atlantic University, Boca Raton, FL 33431, USA
e-mail: hmahfuz@fau.edu

Sandwich panels were then made from nanophased foams and their debond fracture toughnesses were evaluated. The importance of functionalization was also examined.

## Polyurethane foam

A PU foam system reinforced with SiC nanoparticles has been investigated as core material for sandwich structures. The foam consists of polyether polyol with one or more hydroxyl groups (HO–R–OH) attached to the carbon chain (R), and a diisocyanate containing two isocyanate groups (–N=C=O). Diisocyanate reacts with the polyol to form cross-linked PU characterized by its NH–CO–O– groups. The SiC nanoparticles are crystalline with hexagonal lattices of alternating planes of silicon and carbon atoms in their molecular configurations. Thermal oxidation of SiC produced silica ($SiO_2$) on the surface of the nanoparticles which is critical during subsequent functionalization of SiC particles. Exothermic reactions during synthesis of the foam produce segmented blocks of PU which were expanded into foam by co-generation of $CO_2$. Sequential steps in the foaming process are; bubble nucleation, microphase separation, physical gelation, and vitrification of hard segments with interconnecting hydrogen-bonded network. Presence of covalent bonds in SiC influenced the onset of microphase separation and controlled the cell structure of foam. In addition, both PU and SiC molecules have dipole moment which enhances the strength of the covalent bonds and affects the foaming process. The foaming process is explained in a later section.

## Functionalization of SiC nanoparticles

The functionalization of SiC nanoparticles was performed by using a silane coupling agent to enhance bonding between PU and SiC particles. We used organosilanes to modify the surface of SiC nanoparticles. Organosilanes has the ability to incorporate both organic- and inorganic-compatible functionality within the same molecule. The inorganic compatibility comes from the alkoxy groups attached to the silicon atom. This bond is hydrolytically unstable and in the presence of moisture hydrolyses to an intermediate Si–OH bond which then condenses with surface bound OH groups on inorganic surfaces to form stable Si–O–Si bonds. The molecular structure of organosilane and its interaction with inorganic substrates are depicted in Fig. 1. The final step in reacting an organosilane with a substrate is to utilize the substrate to catalyze chemical transformations at the heterogeneous interface, ordering the interface region, and modifying its partition characteristics. Most importantly, it includes the ability to affect covalent

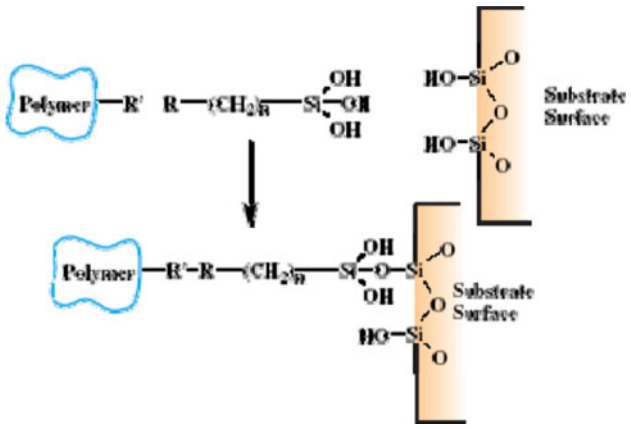


**Fig. 1** Formation of Si–O–Si bond with substrate surface

bonds between the polymer and SiC particles. For any particular chemical bond, the amount of energy it takes to break that bond is exactly the same as the amount of energy released when the bond is formed. This value is called the bond energy. The bond energy of the covalent bonds created between the substrate (SiC particles) and the organofunctional group is very important during the microphase separation stage of the foaming process. In addition, weak secondary bonding forces are created among the covalently bonded molecules due to the presence of permanent dipoles in PU and SiC particles.

Functionalization of SiC particles was performed in the following manner: The weight of SiC nanoparticles that would be necessary for dispersion into Part A of the resin was estimated. Total surface area of SiC particles was then determined using specific surface area (SSA) and estimated weight. Since 1 g of silane (trimethoxysilane) was capable of modifying approximately 358 $m^2$ of inorganic surface, we could estimate the weight of silane required for the particles. Silane was then added through mechanical stirring into a starting mixture of 95% ethanol and 5% water to yield a 2% final concentration of silane. Mixing was conducted for a few minutes to allow hydrolysis and silanol formation. In the next step, nanoparticles were added by stirring them into the silane solution for about 2–3 min. After the particles settled at the bottom, the solution was decanted. Ethanol and water were dried out by heating the particles in a furnace at around 110 °C. If particles were agglomerated, a ball mill was used to bring them back to powder form. The average diameter of nanoparticles was 20–40 nm. SiC nanoparticles were then ready to be dispersed into Part A.

## Foam synthesis and sandwich manufacturing

Part A (isocyanate) of the liquid PU was dispersed with SiC nanoparticles using a mechanical mixer for about

30 min followed by ultrasonic cavitation for another 30 min. SiC particle loading varied from 0.1 to 2.0 wt%. After sonication, Part B (polyol) was added at a ratio of 50:50 by weight through mechanical mixing and was immediately poured into a pre-heated rectangular mold. The mold was closed after pouring the mixture and the polymerization was allowed to complete. Foam panels of thicknesses 12.7 and 25.4 mm were made. The higher thickness foam was used to evaluate debond fracture toughness of sandwich composites. The density of foam was found to be around 80 kg/m$^3$. Samples were also checked under a SEM which revealed a moderate increase in cell dimensions. Several 30 cm × 30 cm sandwich panels were made with the 25.4-mm thick foam core. The face sheets were plain weave carbon fabric with SC-15 epoxy resin. Nine layers of dry fabric preforms were used which eventually produced a face sheet thickness of 2.54 mm. A strip of Teflon tape, 1.27 mm thick and 45 mm long, was inserted at the face/core interface on one side of the panel to introduce initial debond. After the sandwich panels were cured, they were machined into 292-mm long and 25.4-mm wide coupons for TSD testing. Foam specimens were also machined to conduct compression, flexure, and SENB tests. Specimen dimensions will be specified in connection to those tests.

## Mechanical and fracture tests

Mechanical tests were performed to determine compressive, flexural, and fracture properties of the nanophased foams. Compression tests were performed according to ASTM C 365. The specimens were of 25.4 mm × 25.4 mm square cross section. The test was carried out in a Zwick-Roell testing machine equipped with a 50-kN load cell and Test Expert II data acquisition system. Test speed was constant at 2.54 mm/min. Compression tests were conducted using parallel steel plates attached to the grips. Plates were aligned perpendicular to the cross-head motion prior to loading. Three-point flexure tests were conducted per ASTM D 790 using the same Zwick-Roell testing machine. Specimen dimension was 125 mm × 25.4 mm × 12.7 mm. The test fixture had loading nose and supports made of cylindrical surfaces in order to avoid excessive indentation, or failure due to stress concentration directly under the loading nose. At least five replicate specimens were tested in compression and flexure. Flexural strain was calculated from the maximum deflection of the center of the beam assuming linear elastic behavior. Beam deflection was obtained from the cross-head displacement.

Fracture toughness values $K_{IC}$ and $G_{IC}$ were determined using the single-edge-notch bending (SENB) test [25]. SENB test specimens were 112 mm × 25 mm × 12.5 mm

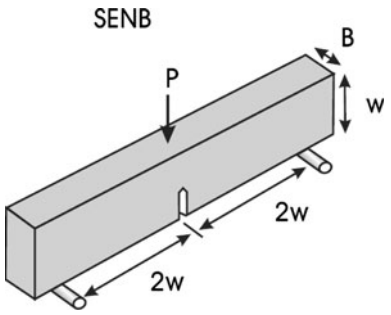


**Fig. 2** Three-point bend SENB test

in dimension and the principle of the test is shown in Fig. 2. Fracture toughness, $K_Q$ was calculated according to ASTM D5045-99:

$$K_Q = \frac{P_Q f(x)}{BW^{1/2}}, \tag{1}$$

where $K_Q$ is the conditional $K_{IC}$, $P_Q$ is the load corresponding to a 5% increased compliance, $W$ is the specimen depth or width, $B$ is the specimen thickness keeping the ratio of $W/B$ equal to two, $a$ is the crack length ($0.45 < a/W < 0.55$), and $f(x)$ is a geometric shape factor, where $x = (a/W)$, and $0 < x < 1$. The following criteria [25] were used to check the validity of the tests:

$$\frac{P_{Max}}{P_Q} < 1.1 \tag{2}$$

$$B, a, (W - a) > 2.5\left(\frac{K_Q}{\sigma_y}\right)^2 \tag{3}$$

If the validity criteria were fulfilled, $K_Q$ was taken as $K_{IC}$. $G_{IC}$ was determined from the area under the load versus displacement curve up to the load $P_Q$ indicated in Fig. 3.

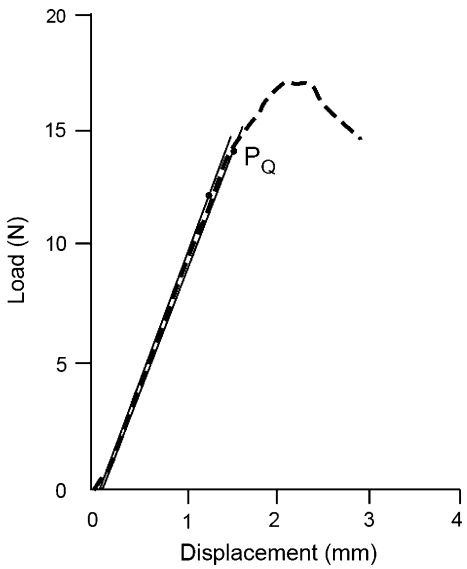


**Fig. 3** Load–displacement curve—SENB test

The energy so obtained, $U_Q$, was corrected for system compliance, loading-pin and support indentation, as specified in ASTM D5045-99 standard. The fracture energy was then corrected for indentation as $U = U_Q - U_i$, and

$$G_Q = \frac{U}{BW\phi}, \tag{4}$$

where $\phi$ is the energy calibration factor given in reference [25], and $U_i$ is the area under the load–displacement graph for the uncracked indentation test specimen.

## Debond fracture toughness test

There is no standard ASTM procedure to determine the debond fracture toughness. Several test specimens have been proposed for this purpose. The tilted sandwich debond (TSD) test was selected for this study. Figure 4 shows the principle of the TSD test. A sandwich specimen with a debond at the upper face/core interface is bonded to a rigid fixture that allows tilting of the specimen. Load is applied to the upper, debonded face until the debond propagates. Typically the TSD specimen is tilted 0° to about 20°. In the current test set up, an aluminum reinforcement plate is adhesively bonded to the top face sheet to reinforce the face sheet to prevent excessive bending deflections. To allow tensile load application to debonded top face sheet, a steel hinge was bonded to the upper face surface. The bottom face of the sandwich was bonded to a steel plate using Loctite quick set epoxy. The specimens had an initial crack length ($a_0$) of 45 mm measured from the loading line. The experimental compliance method was used to determine the debond fracture toughness, $G_c$ [26]. Here a second-order polynomial was fitted to the compliance versus crack length data as:

$$C = m_0 + m_1 a + m_2 a^2 \tag{5}$$

Differentiation of Eq. 5 with respect to crack length provided the fracture toughness,

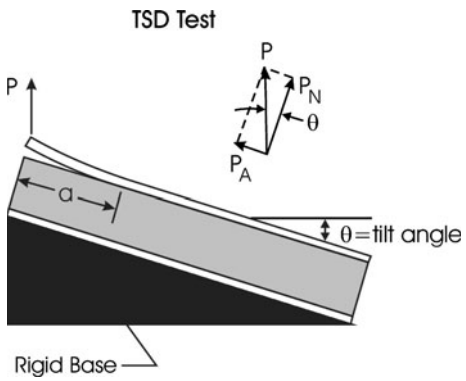


**Fig. 4** TSD test

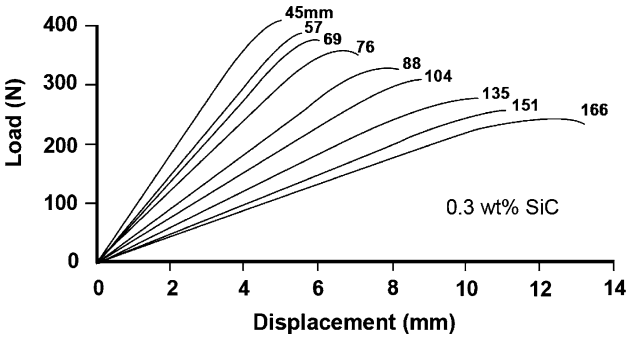


**Fig. 5** Load–displacement curve—TSD test

$$G_c = \frac{P_c^2}{2w}(m_1 + 2m_2 a), \tag{6}$$

where $P_c$ is the critical load at the initiation of debond propagation and $w$ is the width of the specimen.

The specimens were tested in a Zwick-Roell machine at a crosshead speed of 2.5 mm/min. The test began with the recording of load versus deflection data using Zwick data acquisition system while the crack propagation was monitored visually. The initial load was applied for a period until the crack propagated by about 12–15 mm. The specimen was then unloaded completely. In the next step, the specimen was loaded again until the crack propagated another 12–15 mm which was then followed by another unloading. The procedure of loading and unloading continued until the total crack length extended to about 170 mm. This generated a series of load–displacement curves as shown in Fig. 5.

## Results and discussion

### Compression and flexure tests of foams

Representative stress–strain diagrams from compression tests of unreinforced foam, and foams reinforced with 1 wt% SiC particles (nonfunctionalized and functionalized) are shown in Fig. 6. The curves shown in Fig. 6 represent typical compressive behavior of foams as characterized by elastic response up to the yield point followed by a large plastic deformation. This plastic deformation occurs due to the collapse of the cells. Since the density of foam was low, the plastic region was significantly high and accordingly the tests were cut off at around 40% strain without going through the densification stage. The results in Fig. 6 reveal that the compressive yield strength of SiC-infused foam has increased significantly. When SiC particles are functionalized, the enhancement in compressive modulus and strength is elevated further. It is also noticed that yield strain remains almost identical at about 8% in each case

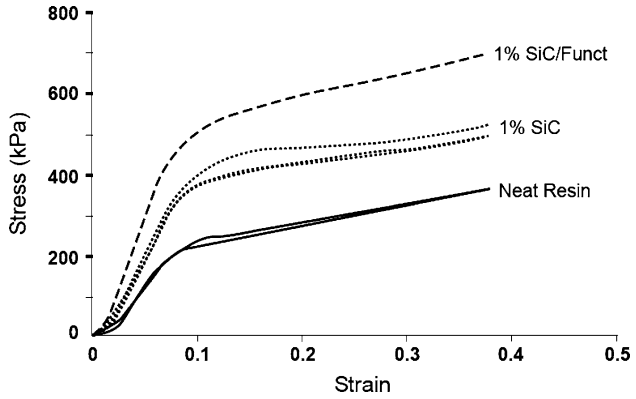


**Fig. 6** Representative stress–strain curves—compression test

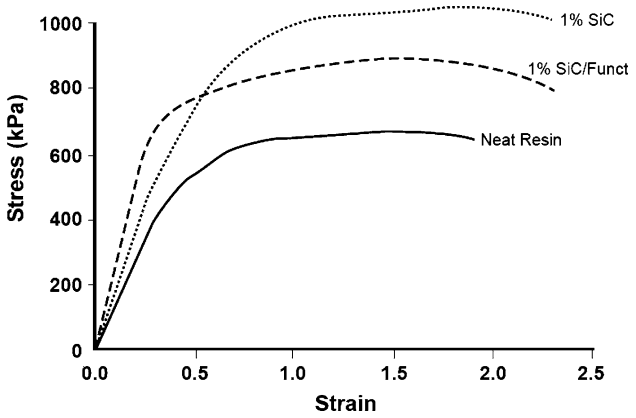


**Fig. 7** Representative stress–strain curves—flexure test

**Table 1** Compression test data for foams

| Sample | Compressive modulus, MPa | Compressive strength, kPa |
|---|---|---|
| Neat foam | 2.58 ± 0.2 | 234 ± 17 |
| 1 wt% SiC | 4.41 ± 0.3 | 448 ± 24 |
| 1 wt% Functionalized SiC | 9.76 ± 0.6 | 689 ± 26 |

**Table 2** Flexural test data for foams

| Sample | Tangent modulus, MPa | Flexural strength, kPa |
|---|---|---|
| Neat foam | 21.5 ± 1.7 | 661 ± 40 |
| 1 wt% SiC | 31 ± 2.7 | 1034 ± 80 |
| 1 wt% Functionalized SiC | 39.6 ± 5.7 | 900 ± 45 |

suggesting that modulus of resilience also increases with particle reinforcement. This increase in energy absorption is similar to what we found earlier with PU foams reinforced with $TiO_2$ particles [5]. Results from compression tests are summarized in Table 1. It is observed in Table 1 that compressive strength and modulus have increased by 92% and 71%, respectively, due to inclusion of 1.0 wt% SiC nanoparticles. After the particles are functionalized, the corresponding enhancements are 194% and 278%, respectively.

Flexural stress–strain diagrams are shown in Fig. 7. Figure 7 shows three curves corresponding to neat, 1.0 wt% SiC, and 1.0 wt% functionalized SiC. The increases in flexural modulus and strength were less than those observed for compression tests. The effect of functionalization in case of flexure was more pronounced with modulus than for the flexural strength. Results are listed in Table 2. Table 2 shows that the gains in flexural strength and modulus with 1.0 wt% concentration were 56% and 44%, respectively. After functionalization, improvement in strength was at 36% while the modulus increased by 84%.

It is observed in both compression and flexure tests that the modulus has increased consistently with the inclusion of SiC particles. We believe such increase in modulus is due to high molecular mixing of Part A with nanoparticles and formation of free radicals which helped faster and efficient cross-linking when Part B was added. This enhanced cross-linking, however, made the nanophased foams more brittle as we will see in the following section.

## Fracture tests of foams

A representative load ($P$) versus loading-point displacement ($\delta$) curve for a 1.0 wt% specimen loaded in three-point flexure SENB fracture test is shown in Fig. 3. Figure 3 shows initial compliance, $C$ and a second line with a compliance 5% greater than that of $C$. Since the maximum load ($P_{max}$) falls outside the second line, the intersection of this line and the $P$–$\delta$ curve is used as $P_Q$ in Eq. 1 to calculate $K_Q$. The $P$–$\delta$ curve displayed some ductility being slightly nonlinear and did not drop to zero load abruptly at the instant of crack growth initiation. The load drop was rather gradual as seen in Fig. 3 suggesting a noncatastrophic failure event. Fracture test results are summarized in Table 3. It is observed that there is about 20–30% reduction in $K_{IC}$ and $G_{IC}$ after SiC particle inclusion. After functionalization of SiC particles, $K_{IC}$ values became similar to that of neat PU, and $G_{IC}$ values were only 11% below the corresponding neat values.

**Table 3** Fracture toughness data for foams

| Sample | Fracture toughness, $K_{IC}$ MPa $m^{1/2}$ | Strain energy release rate, $G_{IC}$, J/$m^2$ |
|---|---|---|
| Neat foam | 0.0836 | 216 |
| 1 wt% SiC | 0.0662 | 146 |
| 1 wt% Functionalized SiC | 0.0822 | 193 |

Although the fracture toughness values of nanophased foams were either below or at the level of neat foams, this demonstrated that functionalized particles performed better than the pristine particles during fracture.

The debond fracture toughness of the sandwich specimens (TSD) was considered next. A set of load–displacement curves for a TSD specimen with 0.3 wt% SiC concentration is shown in Fig. 5. Figure 5 provides the critical load ($P_{cr}$) and compliance, $C$, for each crack length. A fit of the compliance, $C$ versus crack length data, as shown in Fig. 8 provides the relation $C = C(a)$ required for Eq. 5. Each test specimen provided about 8–10 $G_c$ values. A plot of $G_c$ versus crack lengths is shown in Fig. 9. Although Fig. 9 displays a slight increase of $G_c$ over the range of crack lengths examined, it can be stated that debond fracture toughness is not strongly dependent on the crack length. An average value for debond fracture toughness was then calculated and results are listed in Table 4. Data in Table 4 suggest that low concentration of nanoparticles provides a remarkable increase in the debond toughness. At 0.1 wt%, the enhancement in $G_c$ is about 300%. As the concentration of nanoparticles increased over 0.2 wt%, however, $G_c$ decreased but stayed significantly higher than that of the neat. At 1.0 wt% $G_c$, was found to be about 87% more. When the particles were functionalized, $G_c$ also remained high.

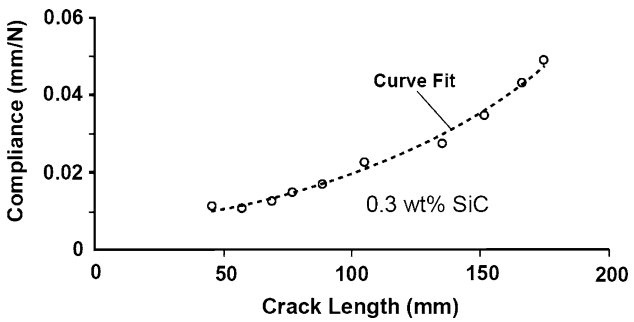


**Fig. 8** Crack length versus compliance curve

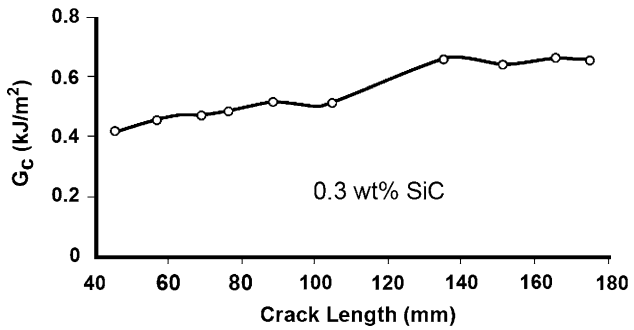


**Fig. 9** Variation of $G_c$ with crack length

**Table 4** Debond fracture toughness for sandwich specimens

| Sample, wt% of SiC | Debond fracture toughness $G_c$, J/m$^2$ |
|---|---|
| Neat | 142 ± 26.8 |
| 0.1 | 561 ± 60 |
| 0.2 | 488 ± 37.5 |
| 0.3 | 337 ± 28 |
| 0.4 | 339 ± 33.9 |
| 1.0 | 265 ± 40.6 |

During debond fracture toughness tests it was observed that cracks propagated in two separate ways as shown in Fig. 10. In the neat and 0.1 wt% specimens, crack propagation occurred right underneath the face with minimum amount of foam adhering to the face (see Fig. 10a and b). On the other hand, in specimens with 1.0 wt% concentration, crack propagation occurred in the foam approximately 1–2 mm underneath the actual face/core interface (see Fig. 10c). This region can be defined as a sub-interface zone which exists between the resin-soaked cells at the top, and dry cells underneath. We believe that the strength of this sub-interface region depends on the strengths of the unfilled and resin-soaked cells. For all cases above 1.0 wt%, it was observed that cracks propagated through this sub-interface region. This sub-interface region has less crack growth resistance than the actual face/core interface.

## Conclusions

Reinforcement of SiC nanoparticles by 1.0 wt% improved the compressive and flexural properties by 50–70% range. With the functionalization of SiC particles, an improvement of the order of 200% was observed. The fracture toughness of the core material is however, somewhat reduced by SiC reinforcement. When nanoparticles are functionalized, fracture toughness can be recovered to the level of neat foam. The debond fracture toughness, $G_c$, increased substantially after addition of small amounts of nanoparticles. Highest enhancement (~300%) was observed at 0.1 wt% SiC. It is evident from the study that enhancement of mechanical and debond fracture toughness does not take place at identical particle concentration, suggesting that reinforcement strategy should be load and application specific. It has been observed that a low-particle concentration (0.1–0.4 wt%) maximize $G_c$ while higher concentrations (~1.0 wt%) provide elevation of the compression and flexure properties. Debond fracture testing further revealed that at high-particle concentrations, the interface crack propagated in the core, away from the actual face/core interface while at lower concentration the crack propagation was very close to the face/core interface.

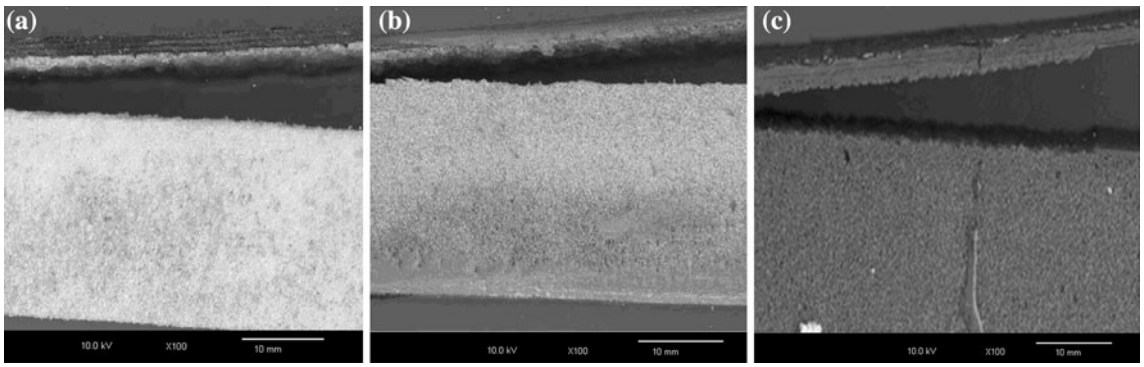


**Fig. 10** Optical Micrographs of fractured interface **a** neat, **b** 0.1 wt%, and **c** 1.0 wt%

**Acknowledgement** We acknowledge with appreciation the support for this work from the Office of Naval Research (ONR) through Grant # N00014-05-1-0341.

## References

1. Mahfuz H, Rangari V, Islam M, Jeelani S (2004) Composites A 35(4):453
2. Mahfuz H, Islam M, Rangari V, Saha M, Jeelani S (2004) Composites B 35:543
3. Hosur MV, Mohammed AA, Zainuddin S, Jeelani S (2008) Mater Sci Eng A 498:100
4. Mohammed AA, Hoosur MV, Jeelani S (2006) Cellular Polym 25(6):293
5. Mahfuz H, Uddin MF, Rangari VK, Saha MC, Zainuddin S, Jeelani S (2005) Appl Compos Mater 12:193
6. Han SH, Do J, Kader MA, Lee JH, Nah C (2004) Polym Adv Technol 15(7):370
7. Rangari V, Watson T, Jeelani S (2006) In: Proceedings of 2006 multifunctional nanocomposites international conference. American Society of Mechanical Engineers, New York. ISBN-10:0791 837858
8. Niuguna J, Michalowski S, Pielichowski K, Walton AC (2008) In: Nanopolymers 2008 conference, 7–8 October 2008, Frankfurt, Germany. Smithers Rapra Ltd., Shrewsbury, UK, 12 pp. ISBN-13:978-1-84735-074-9
9. de Kabin M, Saha MC, Jeelani S (2007) Mater Sci Eng A 459(1–2):111
10. Viana GM, Carlsson LA (2001) Tensile and fracture characterization of PVC Foam Cores, vol 66. American Society of Mechanical Engineers, Aerospace Division (publication) AD, New York, pp 221–224
11. Prasad S, Carlsson LA (1994) Eng Fract Mech 47(6):813
12. Prasad S, Carlsson LA (1994) Eng Fract Mech 47(6):825
13. Carlsson LA, Matteson RC, Aviles F, Loup DC (2005) Compos Sci Technol 65(15–16):2612
14. Marsavina L, Sadowski T (2008) Polym Test 27:941
15. Shiina Y, Hamamoto Y, Okumura K (2006) Europhys Lett 76(4):588
16. Benderly D, Rezek Y, Zafran J, Gorni D (2004) Polym Compos 25(2):229
17. Choi S, Sankar BV (2003) J Compos Mater 37(23):2101
18. Wong SC, Wouterson EM, Boey FYC, Hu X (2005) Compos Sci Technol 65(11–12):1840–1850
19. Saha M, Kabir E, Jeelani S (2008) Mater Lett 62(4–5):567
20. Cotgreave T, Shortall JB (1978) J Mater Sci 13(4):722. doi: 10.1007/BF00570506
21. Wouterson EM, Boey FYC, Wong SC, Chen L, Hu X (2007) Compos Sci Technol 67(14):2924
22. Li X, Carlsson LA (2001) J Compos Mater 35(23):2145
23. Li X, Carlsson LA (1999) On crack extension in TSD specimen with foam core, vol 58. American Society of Mechanical Engineers, Aerospace Division (publication) AD, New York, pp 15–22
24. Johnsen BB, Kinloch AJ, Mohammed RD, Taylor Ac, Sprenger S (2007) Polymer 48:530
25. ASTM D 5045-99, ASTM International, West Conshohocken, PA 19428, USA
26. Li X, Carlsson LA (1999) J Sandwich Struct Mater 1(1):60